Anderson Mobility Gap Probed by Dynamic Coherent Backscattering

L. A. Cobus,[1] S. E. Skipetrov,[2,3] A. Aubry,[4] B. A. van Tiggelen,[2,3] A. Derode,[4] and J. H. Page[1,*]
[1]Department of Physics and Astronomy, University of Manitoba, Winnipeg, Manitoba R3T 2N2, Canada
[2]Université Grenoble Alpes, LPMMC, F-38000 Grenoble, France
[3]CNRS, LPMMC, F-38000 Grenoble, France
[4]Institut Langevin, ESPCI ParisTech, CNRS UMR 7587, Université Denis Diderot—Paris 7, 1 rue Jussieu, 75005 Paris, France
(Received 15 October 2015; published 13 May 2016)

We use dynamic coherent backscattering to study one of the Anderson mobility gaps in the vibrational spectrum of strongly disordered three-dimensional mesoglasses. Comparison of experimental results with the self-consistent theory of localization allows us to estimate the localization (correlation) length as a function of frequency in a wide spectral range covering bands of diffuse transport and a mobility gap delimited by two mobility edges. The results are corroborated by transmission measurements on one of our samples.

DOI: 10.1103/PhysRevLett.116.193901

A quantum particle is trapped in a three-dimensional (3D) disordered potential if its energy E is lower than the so-called mobility edge (ME) E_c. As was discovered by Anderson [1], quantum interferences may increase E_c to values that are much larger than the classical percolation threshold, an energy below which a classical particle would be trapped [2]. The link between E_c and the statistical properties of disorder has been recently studied in experiments with ultracold atoms in random optical potentials [3,4]. In contrast to quantum particles, classical waves—light or sound—may be Anderson localized by disorder only in a band of intermediate energies (or frequencies), the impact of disorder becoming weak in both high- and low-frequency limits [5,6]. One thus expects a mobility "gap" delimited by two MEs instead of a single ME. This is due to the difference between dispersion relations of quantum and classical waves [7,8]. Resonant scattering may further complicate the spectrum by shifting the mobility gap or splitting it into several narrower ones. Mobility gaps can also exist for quantum particles when the disordered potential is superimposed on a periodic one—a common situation for electrons in crystals with impurities [9]. In the present Letter we report the first experimental observation of a mobility gap for classical waves. To this end we take full advantage of experimental techniques available for classical waves but very difficult, if not impossible, to put in practice for quantum particles and, in particular, for electrons in disordered conductors. We perform frequency-, time-, position-, and angle-resolved ultrasonic reflection and transmission experiments in strongly disordered "mesoglasses"—elastic networks of brazed aluminum beads. The results are compared with the self-consistent theory of localization to precisely locate the two MEs and to estimate the localization length ξ throughout the mobility gap. As expected, ξ diverges at the MEs.

Among the many definitions of Anderson localization, two of them rely either on the exponential decay of eigenmodes at large distances or the vanishing of diffusion [10]. However, strictly speaking, both only apply in an infinite disordered medium and not in experiments which involve finite samples with often open boundaries. In the latter case, waves can leak through the sample boundaries to the surrounding medium; hence, the eigenmodes no longer decay exponentially at large distances (because waves propagate freely outside the sample), and the transport is no longer blocked completely, even though wave diffusion is suppressed exponentially. This is why important efforts were devoted in recent years to study signatures of Anderson localization in finite 3D samples that can be seen as representative portions of infinite disordered media in which waves would be Anderson localized. The most impressive successes were achieved for quantities measured in transmission where time- and position-resolved measurements of wave intensity allowed unambiguous observation of Anderson localization of elastic waves [11], without complications due to absorption. However, an important shortcoming of such measurements is the weakness of transmitted signals that decay exponentially with sample thickness L making the regime of very strong localization $L/\xi \gg 1$ inaccessible. Even in the diffuse regime, the transmitted intensity may become so weak that the measured signal is dominated by other, presumably weak phenomena (e.g., nonlinear effects or fluorescence in optics) which can be misinterpreted as a signature of Anderson localization [12,13].

To circumvent the difficulties of transmission experiments, we develop a new approach to Anderson localization of waves based on time- and angle-resolved reflection measurements. The total reflection coefficient of a thick disordered sample is close to unity because almost all the

incident energy is reflected, allowing for comfortable signal levels even deep in the localized regime. For a plane wave incident upon a slab of weakly disordered medium, $k\ell \gg 1$, the average reflection coefficient $R(\theta)$ is known to be almost Lambertian, but with a two-fold enhancement within a narrow angular range $\Delta\theta \sim (k_0\ell^*)^{-1}$ around the exact backscattering direction $\theta = 0$ [14–18]. Here, k and k_0 are the wave numbers inside and outside the sample, respectively, and ℓ and ℓ^* are the scattering and transport mean free paths. If the incident wave is a short pulse, the shape $R(\theta, t)$ of this coherent backscattering (CBS) peak evolves in time, whereas its relative amplitude remains constant [19–21]. The width $\Delta\theta$ of the CBS peak decreases with time according to $\Delta\theta^2 \propto 1/Dt$, where D is the wave diffusion coefficient, as can be easily found from the solution of the diffusion equation [18]. CBS is a very general phenomenon due to constructive interferences of partial waves that follow time-reversed paths in a disordered medium. It was observed for light in suspensions of small dielectric particles [14–16] and clouds of cold atoms [22], sound [20,21], seismic [23], and matter [24] waves. Being an interference phenomenon, CBS seems natural to use as a probe of Anderson localization. However, the stationary (time-integrated) CBS peak was predicted to be only weakly affected by localization effects, with the most pronounced effect being the rounding of its tip, which can also be due to absorption [25]. Optical experiments confirmed the rounding of the tip [26,27], but the conclusion that this behavior was caused by Anderson localization of light [27] was not supported by transmission measurements performed on the same or similar samples [28,29]. In this context, the dynamic CBS is more promising as a probe of Anderson localization because its shape is independent of absorption provided the absorption coefficient is spatially uniform on average, and its width $\Delta\theta$ explicitly depends on the diffusion coefficient D. In a different context, recent theoretical work suggests that dynamic CBS of cold atoms in a random potential may serve as a probe of an Anderson transition [30].

In this Letter we report measurements of CBS from two of our mesoglass samples composed of aluminum beads brazed together (volume fraction ~55%) to form an elastic network. The samples have the shape of slabs with cross sections of 230×250 mm^2 much larger than thicknesses $L_1 = 25 \pm 2$ mm and $L_2 = 38 \pm 2$ mm of samples L1 [see Fig. 1(a)] and L2, respectively. They were waterproofed so that experiments could be performed in a water tank with immersion transducers or transducer arrays, and the pores between the beads held under vacuum during all measurements. The samples are similar to those used in previous studies [11,31], but instead of being monodisperse, they have a mean bead diameter of 3.93 mm with a polydispersity of about 20%, which helps to randomize bead positions. The samples also have stronger elastic bonds between beads than previous samples, visible in Fig. 1(b).

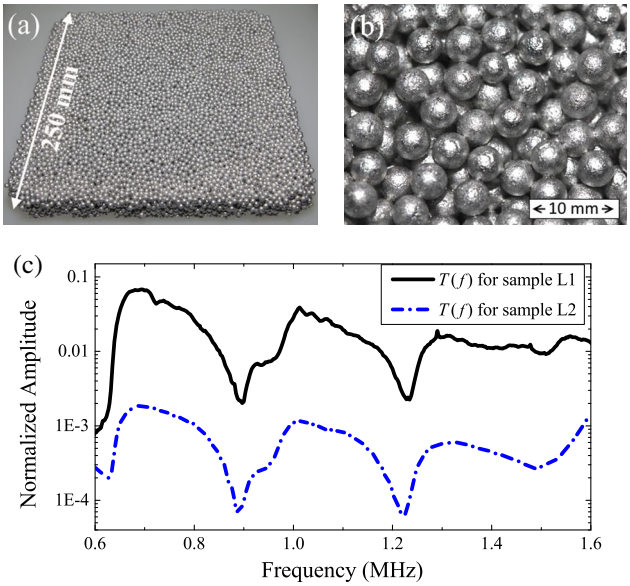

FIG. 1. (a) Sample L1. (b) Bead structure of sample L1. (c) Amplitude transmission coefficient of ultrasonic waves through samples L1 and L2 as a function of frequency.

These differences influence the frequency dependence of the amplitude transmission coefficient, shown in Fig. 1(c). Coupling between the individual resonances of the beads leads to frequency bands of relatively high transmission whose widths depend on the coupling strength [11,32], but these bands are narrow enough in our samples to cause transmission dips to appear in between. The depth and width of the dips are lessened by the polydispersity and greater interbead bond strength compared with the monodisperse samples.

These dips may correspond to Anderson mobility gaps, but one has to study the nature of wave transport in the corresponding frequency ranges to claim anything with certainty. Here, we report a detailed study of wave transport around the transmission dip at 1.23 MHz. Ultrasound is very strongly scattered near this frequency; we have measured the product $k\ell$ as small as $k\ell \lesssim 3$. More details of sample L1 can be found in a previous work [33]. Sample L2 is too thick and too strongly scattering for many of the conventional methods of sample characterization in transmission to work. As no detectable coherent signal could be transmitted through L2 in the frequency range of interest, measurements of k and ℓ from the coherent pulse [34] are not possible. However, both samples were fabricated using the same technique and have very similar composition, so estimates from coherent measurements on sample L1 are expected to be a good approximation for L2 as well.

We measure the backscattered intensity using ultrasonic transducer arrays, placed in the diffuse far field of the samples (for details, see Ref. [35]). A time-dependent "response matrix" was gathered by emitting with each element in turn and recording the time-dependent

backscattered field with all elements [21,33]. An average over configurations of disorder was performed by translating the array parallel to the sample surface and acquiring the response matrices for different positions. To obtain results as a function of both time t and frequency f, the data were filtered using a Gaussian envelope of standard deviation 0.015 MHz, centered around f. As has been previously reported [33], these backscattering data show significant contributions from recurrent scattering due to the signal entering and leaving the sample near the same spot [33,36]. Recurrent scattering complicates the analysis of CBS peaks, as it is difficult to determine the (roughly flat) background intensity level corresponding to large angles θ. The recurrent scattering contribution was removed from the total backscattered intensity following the approach developed previously [33].

To eliminate the effect of absorption, the time-dependent CBS profiles $R(\theta, t)$, where θ is the angle between source and receiver elements of the ultrasonic array, are normalized by $R(0, t)$ [35]. Analogously to transverse confinement measurements in transmission [11], absorption cancels in the ratio $R(\theta, t)/R(0, t)$. Representative profiles $R(\theta, t)/R(0, t)$ are shown in Fig. 2.

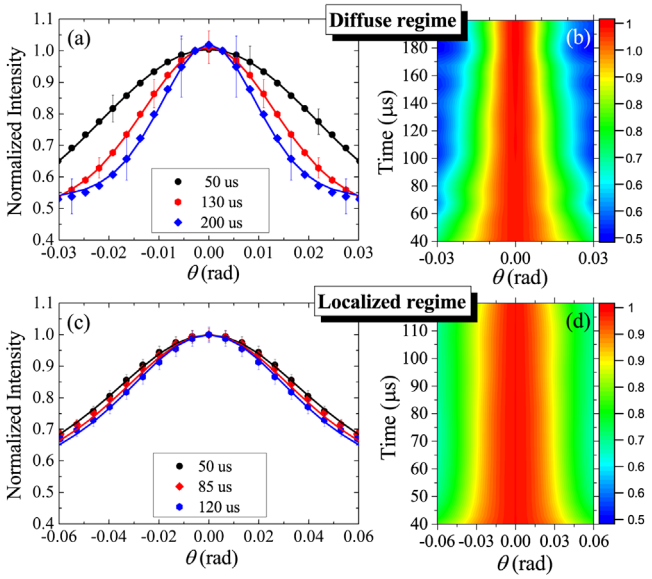

FIG. 2. Dynamic CBS profiles in the diffuse regime (1.65 MHz) (a,b) and in the localized regime (1.22 MHz) (c,d). The results in (a,b) are for sample L1, and in (c,d) for sample L2 (note the different angular scales). In (a,c) theoretical fits (lines) and experimental data (symbols) are shown for three representative times. In (a), the data are fitted using diffusion theory, giving diffusion coefficient $D = D_B = 0.7\ \mathrm{mm}^2/\mu\mathrm{s}$ [37], whereas in (c) SC theory is used, giving $\xi = 16.5$ mm. Additional examples are shown in Ref. [35]. In (b,d) experimental CBS profiles are shown as a function of both time and angle. The profile narrows quite rapidly in the diffuse regime (b) but is almost constant over the accessible range of times in the localized regime (d).

To obtain a quantitative description of our data, we use the self-consistent (SC) theory of Anderson localization with a position-dependent diffusion coefficient $D(z, \Omega)$ presented in Refs. [38,39]. First, $D(z, \Omega)$ is determined from an iterative solution of the self-consistent equations for each depth z inside the sample ($0 \leq z \leq L$). Second, the two-dimensional spatial Fourier transform of the intensity Green's function $C(q_\perp, z, z' = \ell_B^*, \Omega)$ is calculated using this $D(z, \Omega)$. Here, ℓ_B^* is the transport mean free path in the absence of Anderson localization effects. Finally, the CBS profile $R(\theta, t)$ is obtained as a Fourier transform of $R(q_\perp, \Omega) = D(z = 0, \Omega)\partial C(q_\perp, z, z' = \ell_B^*, \Omega)/\partial z|_{z=0}$, where $q_\perp = k_0 \sin\theta$ [35]. Fits to the experimental data obtained from this theory are shown in Fig. 2(c). We refer the reader to Ref. [35] for the details of the fitting procedure. For a given frequency f, important outcomes of the fitting procedure are the location of f with respect to the ME f_c (indicating whether wave transport at f is extended or localized) and the value of the localization length ξ that characterizes the closeness to a ME and the extent of localization effects [40].

CBS profiles shown in Figs. 2(a) and 2(b) exhibit the narrowing with time predicted by the diffusion theory. However, when approaching $f = 1.20$ MHz and beyond, the narrowing of CBS profiles slows down considerably [see Figs. 2(c) and 2(d) and Fig. S1 of Ref. [35]]. This slowing down cannot be described by diffusion theory [35] but is the expected behavior when a ME of the Anderson transition is approached and crossed because the width of the CBS peak $\Delta\theta$ behaves, roughly speaking, as the inverse width of the diffuse halo at the surface of the sample. The latter grows without limit in the diffuse regime but cannot exceed a value on the order of the localization length ξ in the localized regime. Hence, the corresponding CBS profile stops shrinking and its width $\Delta\theta$ saturates. This is illustrated in Fig. 3 where the different types of behavior can be clearly distinguished.

We performed systematic fits of SC theory to our data for frequencies from 1.17 to 1.27 MHz for both samples L1 and L2, thereby determining the frequency dependencies of the localization (correlation) length ξ. The results are shown in Fig. 4 where MEs at approximately 1.20 and 1.24 MHz are indicated by fuzzy vertical gray lines. The Anderson mobility gap is clearly visible in between, whereas the wave transport is subdiffusive for frequencies below 1.20 and above 1.24 MHz. Other and possibly multiple mobility gaps can exist in our samples outside the frequency range from 1.17 to 1.27 MHz that we explored. It is important to note that although the position of the Anderson mobility gap that we have found coincides with one of the dips in the transmission spectra of Fig. 1(c), the latter is not sufficient to claim the existence of the former. Indeed, a dip in transmission can simply correspond to spectral regions with a low density of states—precursors of band gaps in larger samples. It is important to prove that the

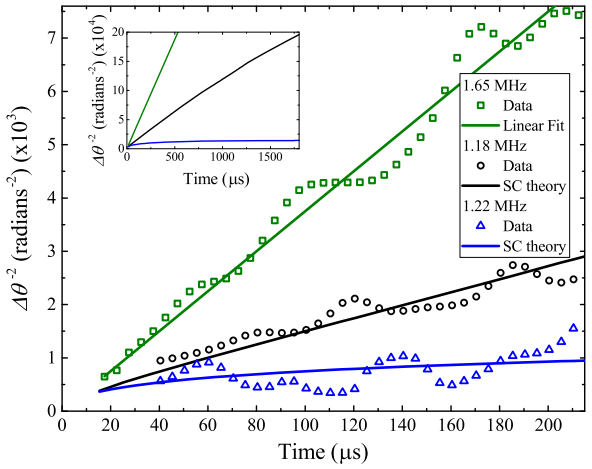

FIG. 3. Experimental results (symbols) and theoretical predictions (lines) for sample L1. Plotted is the reciprocal of the square of the half width at half maximum of the CBS peaks, $\Delta\theta^{-2}(t)$ (error bars are smaller than symbol sizes). Three representative frequencies are shown: $f = 1.65$ MHz (diffuse regime, diffusion coefficient $D_B = 0.7\ \mathrm{mm}^2/\mu\mathrm{s}$ extracted from the fit), $f = 1.18$ MHz (subdiffusion as a ME is approached; correlation length $\xi = 2.1$ mm), and $f = 1.22$ MHz (Anderson localization; localization length $\xi = 12.5$ mm). The inset shows theoretical predictions for longer times.

wave transport corresponds to strongly suppressed diffusion that is consistent with Anderson localization, in order to claim an Anderson mobility gap. This is achieved here by comparing experimental results with SC theory of localization.

To support our conclusions based on CBS measurements, we performed complementary experiments and

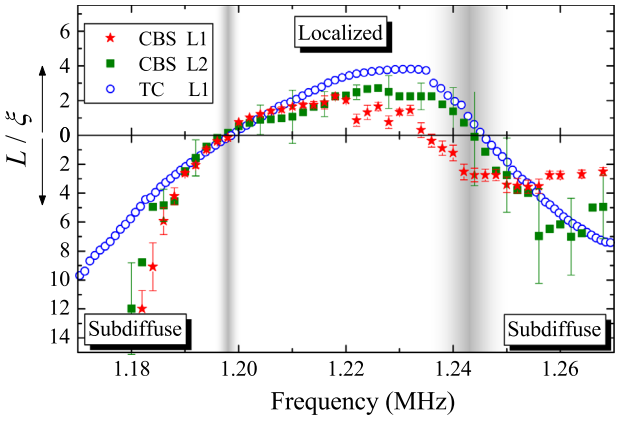

FIG. 4. The ratio of sample thickness L to the localization (correlation) length ξ obtained from fits to experimental CBS profiles (sample L1—red stars, sample L2—green squares) and transverse confinement (TC) data (sample L1—open circles). Error bars represent variations of L/ξ that increase the reduced χ^2 by unity; error bars are smaller than symbol size for transmission results. Fuzzy vertical gray lines show our estimates of mobility edges.

analysis in transmission on sample L1. We used the technique of transverse confinement, which has been previously established as an unambiguous method of observing localization [11]. The experimental method and comparison of measurements with SC theory have been presented in detail in Refs. [11,41,42]. As can be seen in Fig. 4, the results of transmission and reflection experiments agree reasonably well. From the combination of these measurements we estimate the position of MEs to be 1.198 ± 0.001 MHz and 1.243 ± 0.007 MHz. Inside the mobility gap the measured localization length reaches a minimum of 6.5 mm (3.8 times smaller than sample thickness). The CBS results fluctuate much more with frequency, as do the CBS profiles themselves, especially around the upper ME where the position of the ME is less clear than for the lower ME. While large fluctuations are to be expected in this regime, the precision of future measurements could be improved with a greater amount of configurational averaging, longer measurement times, and a wider angular array aperture.

Figure 4 may be used to estimate the critical exponent of the localization transition ν because one expects $\xi(f) \propto |f - f_c|^{-\nu}$ for f in the vicinity of a ME f_c. As can be seen in Fig. 4, L/ξ looks approximately linear as a function of f when it crosses the axis $L/\xi = 0$, leading to $\nu \approx 1$. It should be understood, however, that this result has large uncertainties due to the spread of data points in Fig. 4 (especially at the upper ME). In addition, Fig. 4 is obtained by fitting the experimental data with SC theory, which is known to yield $\nu = 1$ in contradiction with numerical calculations [43] and may thus bias the result. More work is needed to obtain accurate estimates of ν for the localization transitions reported here.

In conclusion, we have employed the dynamic CBS effect to demonstrate an Anderson mobility gap in the spectrum of ultrasound scattered in a 3D strongly disordered elastic network. Performing our measurements in reflection instead of transmission as in previous works [11,31] ensured a sufficiently strong signal throughout the mobility gap, even for a very thick sample. This is a significant advance, as previous experiments were only able to reveal a single mobility edge [31]. Fits to the data by the self-consistent theory of localization yielded precisely the locations of the two mobility edges that serve as bounds of the mobility gap, and the localization length ξ as a function of frequency. We were able to corroborate these results via transmission measurements on one of our samples. This work demonstrates the potential of dynamic CBS experiments to study localization effects in thick samples where transmission measurements are difficult or impossible, allowing us to access the deeply localized regime where $\xi \ll L$. The thickness independence of backscattering in a wide range of times provides an important advantage in the investigation of critical behavior where the elimination of finite-size effects is desired. This

approach, made possible by a combination of modern experimental techniques with a careful theoretical description, can be extended to other classical waves (light, microwaves) as well.

We thank the Agence Nationale de la Recherche for financial support under Grant No. ANR-14-CE26-0032 LOVE and CNRS for support in the framework of a France-Canada PICS project Ultra-ALT. J. H. P. and L. A. C. acknowledge the support of NSERC (Discovery Grant No. RGPIN/9037-2001), the Canada Foundation for Innovation and the Manitoba Research and Innovation Fund (CFI/MRIF, LOF Project No. 23523). A. A. and A. D. benefited from funding by LABEXWIFI (Laboratory of Excellence ANR-10-LABX-24), within the French Program Investments for the Future under Reference No. ANR-10-IDEX-0001-02 PSL*.

*john.page@umanitoba.ca

[1] P. W. Anderson, Phys. Rev. **109**, 1492 (1958).
[2] *50 Years of Anderson Localization*, edited by E. Abrahams (World Scientific, Singapore, 2010).
[3] S. S. Kondov, W. R. McGehee, B. Zirbel, and J. J. DeMarco, Science **334**, 66 (2011).
[4] F. Jendrzejewski, A. Bernard, K. Müller, P. Cheinet, V. Josse, M. Piraud, L. Pezzé, L. Sanchez-Palencia, A. Aspect, and P. Bouyer, Nat. Phys. **8**, 398 (2012).
[5] S. John, Phys. Rev. Lett. **53**, 2169 (1984).
[6] S. John, Phys. Today **44**, No. 5, 32 (1991).
[7] B. A. van Tiggelen, A. Lagendijk, A. Tip, and G. F. Reiter, Europhys. Lett. **15**, 535 (1991).
[8] B. A. van Tiggelen and E. Kogan, Phys. Rev. A **49**, 708 (1994).
[9] P. M. Chaikin and T. C. Lubensky, *Principles of Condensed Matter Physics* (Cambridge University Press, Cambridge, England, 1995).
[10] B. A. van Tiggelen, in *Diffuse Waves in Complex Media*, edited by J. P. Fouque (Kluwer Academic Publishers, Dordrecht, 1999), pp. 1–60.
[11] H. Hu, A. Strybulevych, J. H. Page, S. E. Skipetrov, and B. A. van Tiggelen, Nat. Phys. **4**, 945 (2008).
[12] T. Sperling, L. Schertel, M. Ackermann, G. Aubry, C. M. Aegerter, and G. Maret, New J. Phys. **18**, 013039 (2016).
[13] S. E. Skipetrov and J. H. Page, New J. Phys. **18**, 021001 (2016).
[14] Y. Kuga and A. Ishumaru, J. Opt. Soc. Am. A **1**, 831 (1984).
[15] M. P. Van Albada and A. Lagendijk, Phys. Rev. Lett. **55**, 2692 (1985).
[16] P. E. Wolf and G. Maret, Phys. Rev. Lett. **55**, 2696 (1985).
[17] E. Akkermans, P. E. Wolf, and R. Maynard, Phys. Rev. Lett. **56**, 1471 (1986).
[18] E. Akkermans and G. Montambaux, *Mesoscopic Physics of Electrons and Photons* (Cambridge University Press, Cambridge, England, 2007).
[19] R. Vreeker, M. Van Albada, R. Sprik, and A. Lagendijk, Phys. Lett. A **132**, 51 (1988).
[20] G. Bayer and T. Niederdränk, Phys. Rev. Lett. **70**, 3884 (1993).
[21] A. Tourin, A. Derode, P. Roux, B. A. van Tiggelen, and M. Fink, Phys. Rev. Lett. **79**, 3637 (1997).
[22] G. Labeyrie, F. de Tomasi, J.-C. Bernard, C. A. Müller, C. Miniatura, and R. Kaiser, Phys. Rev. Lett. **83**, 5266 (1999).
[23] E. Larose, L. Margerin, B. A. van Tiggelen, and M. Campillo, Phys. Rev. Lett. **93**, 048501 (2004).
[24] F. Jendrzejewski, K. Müller, J. Richard, A. Date, T. Plisson, P. Bouyer, A. Aspect, and V. Josse, Phys. Rev. Lett. **109**, 195302 (2012).
[25] B. A. van Tiggelen, A. Lagendijk, and D. S. Wiersma, Phys. Rev. Lett. **84**, 4333 (2000).
[26] D. S. Wiersma, P. Bartolini, A. Lagendijk, and R. Righini, Nature (London) **390**, 671 (1997).
[27] F. J. P. Schuurmans, M. Megens, D. Vanmaekelbergh, and A. Lagendijk, Phys. Rev. Lett. **83**, 2183 (1999).
[28] T. van der Beek, P. Barthelemy, P. M. Johnson, D. S. Wiersma, and A. Lagendijk, Phys. Rev. B **85**, 115401 (2012).
[29] J. Gómez Rivas, R. Sprik, A. Lagendijk, L. D. Noordam, and C. W. Rella, Phys. Rev. E **63**, 046613 (2001).
[30] S. Ghosh, D. Delande, C. Miniatura, and N. Cherroret, Phys. Rev. Lett. **115**, 200602 (2015).
[31] W. K. Hildebrand, A. Strybulevych, S. E. Skipetrov, B. A. van Tiggelen, and J. H. Page, Phys. Rev. Lett. **112**, 073902 (2014).
[32] J. A. Turner, M. Chambers, and R. L. Weaver, Acustica **84**, 628 (1998).
[33] A. Aubry, L. A. Cobus, S. E. Skipetrov, B. A. van Tiggelen, A. Derode, and J. H. Page, Phys. Rev. Lett. **112**, 043903 (2014).
[34] J. H. Page, P. Sheng, H. P. Schriemer, and I. Jones, Science **271**, 634 (1996).
[35] See Supplemental Material at http://link.aps.org/supplemental/10.1103/PhysRevLett.116.193901 for details of our theoretical model and fitting procedure.
[36] D. Wiersma, M. P. van Albada, B. A. van Tiggelen, and A. Lagendijk, Phys. Rev. Lett. **74**, 4193 (1995).
[37] The diffusion theory used here (to be published in a future work) is for acoustic waves in a 3D medium, similar to that presented for 2D in Ref. [21].
[38] S. E. Skipetrov and B. A. van Tiggelen, Phys. Rev. Lett. **96**, 043902 (2006).
[39] N. Cherroret and S. E. Skipetrov, Phys. Rev. E **77**, 046608 (2008).
[40] ξ plays the role of correlation length in the diffuse regime.
[41] J. H. Page, in *Nano Optics and Atomics: Transport of Light and Matter Waves*, edited by R. Kaiser, D. Wiersma, and L. Fallani (International School of Physics "Enrico Fermi," Course CLXXIII, IOS, Amsterdam; SIF, Bologna, 2011), pp. 95–114.
[42] W. K. Hildebrand, Doctoral thesis, University of Manitoba (2015), http://mspace.lib.umanitoba.ca/handle/1993/30843.
[43] K. Slevin and T. Ohtsuki, New J. Phys. **16**, 015012 (2014).